ELSEVIER

Comput. Methods Appl. Mech. Engrg. 190 (2001) 4831–4846

Computer methods in applied mechanics and engineering

www.elsevier.com/locate/cma

Numerical simulations of fracture problems by coupling the FEM and the direct method of lines

Weizhu Bao *, Houde Han, Zhongyi Huang

Department of Applied Mathematics, Tsinghua University, Beijing 100084, People's Republic of China

Received 28 May 1999; received in revised form 18 January 2000

Abstract

In this paper, we propose a method for calculating stress intensity factors of plane fracture problems with cracks by coupling the finite element method (FEM) and the direct method of lines. We introduce polygonal artificial boundaries and divide the physical domain into two parts: a large domain without any crack tips and small polygonal domains surrounding the crack tips. We solve the problem defined in the small domains with crack tips by using the direct method of lines and design discrete nonlocal artificial boundary conditions on the polygonal artificial boundaries by imposing the continuity of displacement and normal stress. Then the original problem is reduced to a boundary value problem defined in a domain without any crack tips. The finite element approximation of the reduced problem is considered and we can prove that the finite element approximation is well posed. Numerical examples and results of a fracture problem with exact solution and two typical fracture problems demonstrate the efficiency and accuracy of the present method.

Keywords: Finite element method (FEM); Direct method of lines; Stress intensity fractors; Fracture problems

1. Introduction

On a bounded polygonal domain $\Omega \subset \mathbb{R}^2$ containing a single edge crack (see Fig. 1), we consider a boundary value problem of Navier's equations:

$$-\mu\Delta u - (\lambda+\mu)\text{grad div}\, u = f \quad \text{in } \Omega, \tag{1.1}$$

$$u = g \quad \text{on } \Gamma_1, \tag{1.2}$$

$$\sum_{j=1}^{2} \sigma_{ij}(u) n_j = q_i \quad \text{on } \Gamma_2, \ \ 1 \leqslant i \leqslant 2, \tag{1.3}$$

where $u = (u_1, u_2)^{\mathrm{T}}$ denotes the displacement, λ, μ are Lamé constants of the material, $\partial\Omega = \Gamma_1 \cup \Gamma_2$ and $OP, OQ \subset \Gamma_2$ (see Fig. 1); $n = (n_1, n_2)^{\mathrm{T}}$ is the outward normal derivative, $f = (f_1, f_2)^{\mathrm{T}}$, $g = (g_1, g_2)^{\mathrm{T}}$ and $q = (q_1, q_2)^{\mathrm{T}}$ are given functions and satisfy: $f \equiv 0$ in a neighborhood of the crack tip O and $q = 0$ on the segments OP and OQ; $\sigma(u) = (\sigma_{ij}(u))_{2\times 2}$ is the stress tensor with entries:

* Corresponding author. Present address: School of Mathematics, Georgia Institute of Technology, Atlanta, GA 30332-0160, USA.
E-mail address: wbao@math.gatech.edu (W. Bao).

0045-7825/01/$ - see front matter
PII: S0045-7825(00)00351-0

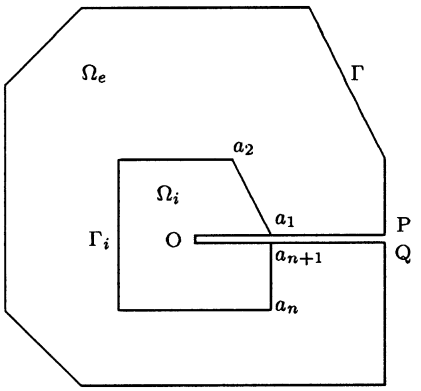

Fig. 1. Set up of physical domain and artificial boundary.

$$\sigma_{ij}(u) = \lambda\delta_{ij}\operatorname{div} u + \mu\left(\frac{\partial u_i}{\partial x_j} + \frac{\partial u_j}{\partial x_i}\right) \quad 1 \leqslant i,\ \ j \leqslant 2. \tag{1.4}$$

It is well known that the solution of the problem (1.1)–(1.3) possesses singularity at the crack tip O [1]. Hence the conventional finite element method (FEM) or finite difference method does not work very well. The problem is that a finite number of these elements cannot represent the transition from infinite stresses at the crack tip to finite stresses elsewhere. To overcome this difficulty and improve accuracy, a number of methods were proposed in the last two decades. For instances, Holston [2] and Cai et al. [3] designed a number of special crack tip elements with the proper singularities (especially for plane problems) and coupled them with the usual finite elements outside a small region that is around the crack tip to solve many problems. Thatcher [4], Ying [5] and Han et al. [6] proposed the infinite element method to deal with singularities. Babuška et al. [7], Akin [8], Whiteman et al. [9] used the standard FEM with local mesh refinement technique to solve problems with singularities. Cheung et al. [10] developed the finite strip method to solve plane fracture problems. Givoli et al. [11–13] and Wu et al. [14] presented a method through designing an artificial boundary condition at a *circle* or a *circular arc* artificial boundary to solve some elliptic boundary value problems in domains with singularities. Since their artificial boundary is a circle or circular arc, thus the remained computational domain has a curved boundary. One must either use elements with curved sides or approximate the circle by a polygonal line when one uses finite element method to solve the reduced problem. The former makes the computation complicated and the later introduces additional numerical error. Recently we developed a method called the direct method of lines to solve problems in unbounded domains and in bounded domain with singularities [15–18]. The artificial boundaries we introduced are *polygonal lines*. Thus the remained computational domain is a polygon. One can apply finite element method easily after designing the artificial boundary conditions properly. Another benefit is that we need not know the degree of singularity priorly. This gives us opportunity to apply our method to a lot of problems where the theoretical expansion of the solution near the tips is unknown. Other approaches may be found in [19–21] and the references therein.

In this paper, we applied our approach to numerical simulations of fracture problems. We introduce a polygonal line artificial boundary $\Gamma_i = \overline{a_1 a_2 \cdots a_{n+1}}$ which divides the domain Ω into two parts, Ω_i and Ω_e satisfying $f \equiv 0$ in Ω_i (see Fig. 1). In the region around the crack tip, Ω_i, we use the direct method of lines that is a semi-discrete approach and related to the method of lines [22] to discretize the problem and design an artificial boundary condition at the polygonal line boundary Γ_i by imposing the continuity of displacement and normal stress at Γ_i. In Ω_e, we apply the usual finite element method using the artificial boundary condition designed at Γ_i to get an approximation. Of course, the artificial boundary condition we designed is nonlocal, this will introduce a full block in the stiffness matrix, see also [23]. Since this full block is only related to the nodes on Γ_i and the number of nodes on Γ_i (Γ_i is a one-dimensional line) is much less than the total number of nodes on Ω_e (Ω_e is a two-dimensional polygon), the additional cost for solving the corresponding linear system is less than 10% of that for solving a system without the full block,

see a detail discussion in [23]. Numerical examples are given and results are compared with the exact solution and previous results to demonstrate the efficiency and accuracy of the present method. Although only the formulation for the problem (1.1)–(1.3) is presented, it is obvious that many other fracture problems of practical importance, e.g., problems in domains with multi-cracks or complex geometry, can be formulated in a similar manner. As the present method combines the advantages of the flexibility of the standard finite element method and the high accuracy of the direct method of lines in the region around the crack tip, Ω_i, this method offers an efficient approach for fracture problems, especially for composite materials.

The layout of this paper is as follows. In the next section, we use the direct method of lines to discretize the problem (1.1)–(1.3) in the domain Ω_i and design a discrete artificial boundary condition at Γ_i for the solution u. In Section 3, we approximate the original problem in the domain Ω_e by the finite element method using the discrete artificial boundary condition designed in Section 2. In Section 4, we present the numerical implementation of coupling the FEM and the direct method of lines. In Section 5 we report three numerical examples, which demonstrate the efficiency of the present method. In Section 6 some discussions and conclusions are given. Guidelines to choosing the shape and size of the artificial boundary Γ_i are also addressed.

2. The direct method of lines

We introduce a Cartesian coordinate system (x_1, x_2) such that the segment OP coincides with the x_1 axis and the corresponding polar coordinate system is (r, θ). Suppose the coordinate of the vertex a_i is $(x_1^i, x_2^i) = (R_i \cos\theta_i, R_i \sin\theta_i)$ for $i = 1, 2, \ldots, n+1$ satisfying $0 = \theta_1 < \theta_2 < \cdots < \theta_{n+1} = 2\pi$. Then for $i = 1, 2, \ldots, n$ the equation of the line coinciding with the segment $\overline{a_i a_{i+1}}$ is

$$x_2 - x_2^i = \frac{\left(x_2^{i+1} - x_2^i\right)}{\left(x_1^{i+1} - x_1^i\right)}\left(x_1 - x_1^i\right) \tag{2.1}$$

or in polar coordinate

$$r = \frac{x_2^i\left(x_1^{i+1} - x_1^i\right) - x_1^i\left(x_2^{i+1} - x_2^i\right)}{\sin\theta\left(x_1^{i+1} - x_1^i\right) - \cos\theta\left(x_2^{i+1} - x_2^i\right)} \equiv \frac{\rho_i}{\sin(\theta - \alpha_i)}, \tag{2.2}$$

where

$$\rho_i = \frac{x_1^{i+1}x_2^i - x_1^i x_2^{i+1}}{|\overline{a_i a_{i+1}}|}, \quad |\overline{a_i a_{i+1}}| = \sqrt{\left(x_1^{i+1} - x_1^i\right)^2 + \left(x_2^{i+1} - x_2^i\right)^2}, \tag{2.3}$$

$$\sin\alpha_i = \frac{x_2^{i+1} - x_2^i}{|\overline{a_i a_{i+1}}|}, \quad \cos\alpha_i = \frac{x_1^{i+1} - x_1^i}{|\overline{a_i a_{i+1}}|}. \tag{2.4}$$

Thus, we introduce the transformation on each triangle D_i with vertexes a_i, O and a_{i+1} for $i = 1, 2, \ldots, n$ (see Fig. 2)

$$x_1 = \frac{\rho_i e^{\rho}\cos\phi}{\sin(\phi - \alpha_i)}, \qquad x_2 = \frac{\rho_i e^{\rho}\sin\phi}{\sin(\phi - \alpha_i)}, \quad \theta_i \leqslant \phi \leqslant \theta_{i+1}, \ -\infty \leqslant \rho < 0. \tag{2.5}$$

It is straightforward to check that the transformation (2.5) maps the triangle D_i onto a semi-infinite strip $\tilde{D}_i = \{(\rho, \phi) \mid \theta_i < \phi < \theta_{i+1}, \ -\infty < \rho < 0\}$ and the segment $\overline{a_i a_{i+1}}$ onto a segment $\{(0, \phi) \mid \theta_i \leqslant \phi \leqslant \theta_{i+1}\}$. Thus the domain Ω_i is mapped onto $\tilde{\Omega}_i = \{(\rho, \phi) \mid 0 < \phi < 2\pi, \ -\infty < \rho < 0\}$ and Γ_i is mapped onto$\tilde{\Gamma}_i = \{(0, \phi) \mid 0 \leqslant \phi \leqslant 2\pi\}$. Furthermore on each D_i, we have that

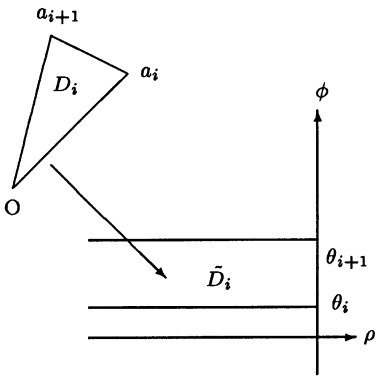

Fig. 2. Transformation between triangle D_i and semi-infinite strip $\tilde{D}_i$.

$$\frac{\partial}{\partial x_1} = -\rho_i^{-1}\mathrm{e}^{-\rho}\left[\sin\alpha_i\frac{\partial}{\partial\rho} + \sin\phi\sin(\phi-\alpha_i)\frac{\partial}{\partial\phi}\right],$$
$$\frac{\partial}{\partial x_2} = \rho_i^{-1}\mathrm{e}^{-\rho}\left[\cos\alpha_i\frac{\partial}{\partial\rho} + \cos\phi\sin(\phi-\alpha_i)\frac{\partial}{\partial\phi}\right]. \tag{2.6}$$

Let

$$X_{\theta_i^+} = (\sin\theta_i\sigma_{11} - \cos\theta_i\sigma_{12})|_{\phi=\theta_i^+}, \qquad Y_{\theta_i^+} = (\sin\theta_i\sigma_{21} - \cos\theta_i\sigma_{22})|_{\phi=\theta_i^+}, \quad 1\leqslant i\leqslant n, \tag{2.7}$$

$$X_{\theta_i^-} = (\sin\theta_i\sigma_{11} - \cos\theta_i\sigma_{12})|_{\phi=\theta_i^-}, \qquad Y_{\theta_i^-} = (\sin\theta_i\sigma_{21} - \cos\theta_i\sigma_{22})|_{\phi=\theta_i^-}, \quad 2\leqslant i\leqslant n+1, \tag{2.8}$$

$$X_n = (-\sin\alpha_i\sigma_{11} + \cos\alpha_i\sigma_{12})|_{\rho=0}, \qquad Y_n = (-\sin\alpha_i\sigma_{21} + \cos\alpha_i\sigma_{22})|_{\rho=0}, \quad \theta_i\leqslant\phi\leqslant\theta_{i+1}. \tag{2.9}$$

Here $(X_{\theta_i^+},\ Y_{\theta_i^+})$ and $(X_{\theta_i^-},\ Y_{\theta_i^-})$ denote the normal stresses at the segment $\overline{Oa_i}$ in the triangles D_i and D_{i-1}, respectively; (X_n, Y_n) denotes the normal stress at the segment $\overline{a_ia_{i+1}}$ in the triangle D_i. From (1.4), (2.6) and (2.9) we have

$$\begin{aligned} X_n &= (-\sin\alpha_i\sigma_{11} + \cos\alpha_i\sigma_{12})|_{\rho=0} \\ &= \frac{1}{\rho_i}\left[\left[\mu + (\lambda+\mu)\sin^2\alpha_i\right]\frac{\partial u_1}{\partial\rho} + \sin(\phi-\alpha_i)[\mu\cos\phi\cos\alpha_i + (\lambda+2\mu)\sin\phi\sin\alpha_i]\frac{\partial u_1}{\partial\phi}\right. \\ &\quad \left. - \frac{\lambda+\mu}{2}\sin 2\alpha_i\frac{\partial u_2}{\partial\rho} - \sin(\phi-\alpha_i)(\lambda\sin\alpha_i\cos\phi + \mu\cos\alpha_i\sin\phi)\frac{\partial u_2}{\partial\phi}\right]_{\rho=0}, \quad \theta_i\leqslant\phi\leqslant\theta_{i+1}, \end{aligned} \tag{2.10}$$

$$\begin{aligned} Y_n &= (-\sin\alpha_i\sigma_{21} + \cos\alpha_i\sigma_{22})|_{\rho=0} \\ &= \frac{1}{\rho_i}\left[-\frac{\lambda+\mu}{2}\sin 2\alpha_i\frac{\partial u_1}{\partial\rho} - \sin(\phi-\alpha_i)(\mu\sin\alpha_i\cos\phi + \lambda\cos\alpha_i\sin\phi)\frac{\partial u_1}{\partial\phi}\right. \\ &\quad \left. + \left[\mu + (\lambda+\mu)\cos^2\alpha_i\right]\frac{\partial u_2}{\partial\rho} + \sin(\phi-\alpha_i)[\mu\sin\phi\sin\alpha_i + (\lambda+2\mu)\cos\phi\cos\alpha_i]\frac{\partial u_2}{\partial\phi}\right]_{\rho=0}, \quad \theta_i\leqslant\phi\leqslant\theta_{i+1}. \end{aligned} \tag{2.11}$$

Combining (1.1)–(1.3), (2.5) and (2.6), the problem (1.1)–(1.3) in the domain Ω_i is reduced to the following discontinuous coefficient problem on the semi-infinite strip $\tilde{\Omega}_i$ in the new coordinate (ρ, ϕ):

$$\frac{\mu+(\lambda+\mu)\sin^2\alpha_i}{\sin^2(\phi-\alpha_i)}\frac{\partial^2 u_1}{\partial\rho^2}+\frac{\mu\cos\phi\cos\alpha_i+(\lambda+2\mu)\sin\phi\sin\alpha_i}{\sin(\phi-\alpha_i)}\frac{\partial^2 u_1}{\partial\rho\partial\phi}-\frac{(\lambda+\mu)\sin 2\alpha_i}{2\sin^2(\phi-\alpha_i)}\frac{\partial^2 u_2}{\partial\rho^2}$$
$$-\frac{\mu\sin\phi\cos\alpha_i+\lambda\cos\phi\sin\alpha_i}{\sin(\phi-\alpha_i)}\frac{\partial^2 u_2}{\partial\rho\partial\phi}+\frac{\partial}{\partial\phi}\left\{\frac{(\lambda+2\mu)\sin\phi\sin\alpha_i+\mu\cos\phi\cos\alpha_i}{\sin(\phi-\alpha_i)}\frac{\partial u_1}{\partial\rho}\right.$$
$$\left.+\left[\mu+(\lambda+\mu)\sin^2\phi\right]\frac{\partial u_1}{\partial\phi}-\frac{\mu\cos\phi\sin\alpha_i+\lambda\sin\phi\cos\alpha_i}{\sin(\phi-\alpha_i)}\frac{\partial u_2}{\partial\rho}-\frac{\lambda+\mu}{2}\sin 2\phi\frac{\partial u_2}{\partial\phi}\right\}=0,$$
$$\theta_i<\phi<\theta_{i+1},\quad -\infty<\rho<0,\quad 1\leqslant i\leqslant n, \tag{2.12}$$

$$-\frac{(\lambda+\mu)\sin 2\alpha_i}{2\sin^2(\phi-\alpha_i)}\frac{\partial^2 u_1}{\partial\rho^2}-\frac{\lambda\sin\phi\cos\alpha_i+\mu\cos\phi\sin\alpha_i}{\sin(\phi-\alpha_i)}\frac{\partial^2 u_1}{\partial\rho\partial\phi}+\frac{\mu+(\lambda+\mu)\cos^2\alpha_i}{\sin^2(\phi-\alpha_i)}\frac{\partial^2 u_2}{\partial\rho^2}$$
$$+\frac{\mu\sin\phi\sin\alpha_i+(\lambda+2\mu)\cos\phi\cos\alpha_i}{\sin(\phi-\alpha_i)}\frac{\partial^2 u_2}{\partial\rho\partial\phi}+\frac{\partial}{\partial\phi}\left\{-\frac{\lambda\cos\phi\sin\alpha_i+\mu\sin\phi\cos\alpha_i}{\sin(\phi-\alpha_i)}\frac{\partial u_1}{\partial\rho}\right.$$
$$\left.-\frac{\lambda+\mu}{2}\sin 2\phi\frac{\partial u_1}{\partial\phi}+\frac{\mu\sin\phi\sin\alpha_i+(\lambda+2\mu)\cos\phi\cos\alpha_i}{\sin(\phi-\alpha_i)}\frac{\partial u_2}{\partial\rho}+\left[\mu+(\lambda+\mu)\cos^2\phi\right]\frac{\partial u_2}{\partial\phi}\right\}=0,$$
$$\theta_i<\phi<\theta_{i+1},\quad -\infty<\rho<0,\quad 1\leqslant i\leqslant n, \tag{2.13}$$

$$u(\rho,\theta_i^+)=u(\rho,\theta_i^-),\quad -\infty\leqslant\rho<0,\quad 1<i\leqslant n, \tag{2.14}$$

$$X_{\theta_i^+}=X_{\theta_i^-},\qquad Y_{\theta_i^+}=Y_{\theta_i^-},\quad -\infty\leqslant\rho<0,\quad 1<i\leqslant n, \tag{2.15}$$

$$X_{\theta_1^+}=Y_{\theta_1^+}=X_{\theta_{n+1}^-}=Y_{\theta_{n+1}^-}=0,\quad -\infty\leqslant\rho<0, \tag{2.16}$$

$$u|_{\rho=0}=u^0(\phi),\quad 0\leqslant\phi\leqslant 2\pi, \tag{2.17}$$

$$u \text{ is bounded}\quad \text{when } \rho\to-\infty, \tag{2.18}$$

where $u^0(\phi)=u|_{\Gamma_i}$.

Let $H^1(0,2\pi)$ denote the usual Sobolev space on the interval $(0,2\pi)$. Furthermore we introduce

$$W_1=H^1(0,2\pi),\quad W=W_1\times W_1,$$

$$V_1=\left\{v_1(\rho,\phi)\mid \text{for fixed } \rho\in(-\infty,0],\ v_1,\frac{\partial v_1}{\partial\rho},\frac{\partial^2 v_1}{\partial\rho^2}\in W_1\right\},$$

$$V=V_1\times V_1.$$

Then the boundary value problem (2.12)–(2.18) is equivalent to the following variational-differential problem:

Find $u(\rho,\phi)\in V$ such that

$$\frac{\mathrm{d}^2}{\mathrm{d}\rho^2}A_2(u,v)+\frac{\mathrm{d}}{\mathrm{d}\rho}A_1(u,v)+A_0(u,v)=0\quad\forall v\in W,\ -\infty<\rho<0, \tag{2.19}$$

$$u|_{\rho=0}=u^0(\phi),\quad 0\leqslant\phi\leqslant 2\pi, \tag{2.20}$$

$$u \text{ is bounded}\quad \text{when } \rho\to-\infty, \tag{2.21}$$

where

$$A_2(u,v)=\sum_{i=1}^{n}\int_{\theta_i}^{\theta_{i+1}}\frac{v(\phi)^{\mathrm{T}}\mathbb{K}_1(\alpha_i)u(\rho,\phi)}{\sin^2(\phi-\alpha_i)}\,\mathrm{d}\phi, \tag{2.22}$$

$$A_1(u,v)=\sum_{i=1}^{n}\int_{\theta_i}^{\theta_{i+1}}\frac{1}{\sin(\phi-\alpha_i)}\left[v(\phi)^{\mathrm{T}}\mathbb{K}_2^i\frac{\partial u(\rho,\phi)}{\partial\phi}-v'(\phi)^{\mathrm{T}}(\mathbb{K}_2^i)^{\mathrm{T}}u(\rho,\phi)\right]\mathrm{d}\phi, \tag{2.23}$$

$$A_0(u,v)=-\int_0^{2\pi}v'(\phi)^{\mathrm{T}}\mathbb{K}_1(\phi)\frac{\partial u(\rho,\phi)}{\partial\phi}\,\mathrm{d}\phi \tag{2.24}$$

with

$$\mathbb{K}_1(\psi)=\begin{pmatrix}\mu+(\lambda+\mu)\sin^2\psi & -\frac{\lambda+\mu}{2}\sin 2\psi\\ -\frac{\lambda+\mu}{2}\sin 2\psi & \mu+(\lambda+\mu)\cos^2\psi\end{pmatrix},$$

$$\mathbb{K}_2^i=\begin{pmatrix}\mu\cos\phi\cos\alpha_i+(\lambda+2\mu)\sin\phi\sin\alpha_i & -\mu\sin\phi\cos\alpha_i-\lambda\cos\phi\sin\alpha_i\\ -\mu\cos\phi\sin\alpha_i-\lambda\sin\phi\cos\alpha_i & \mu\sin\phi\sin\alpha_i+(\lambda+2\mu)\cos\phi\cos\alpha_i\end{pmatrix}.$$

Now, we consider a semi-discrete approximation of problem (2.19)–(2.21). Assume that

$$0=\phi_1<\phi_2<\cdots<\phi_M=2\pi$$

is a partition of the interval $[0,2\pi]$ and for every θ_i, $(i=1,2,\ldots,n+1)$ there is a ϕ_j such that $\phi_j=\theta_i$. Let $h=\max_{1\leqslant j\leqslant M-1}(\phi_{j+1}-\phi_j)$ and

$$W_1^h=\left\{v_1^h(\phi)\in W_1: v_1^h(\phi)|_{[\phi_j,\phi_{j+1}]}\in P_1([\phi_j,\phi_{j+1}]),\ 1\leqslant j\leqslant M-1\right\},$$

$$V_1^h=\left\{v_1^h(\rho,\phi)\in V_1:\text{ for fixed }\rho\in(-\infty,0],\ v_1^h,\frac{\partial v_1^h}{\partial\rho},\frac{\partial^2 v_1^h}{\partial\rho^2}\in W_1^h\right\},$$

$$W_h=W_1^h\times W_1^h,\quad V_h=V_1^h\times V_1^h.$$

Then we obtain a semi-discrete formulation of problem (2.19)–(2.21):

Find $u_h(\rho,\phi)\in V_h$ such that

$$\frac{\mathrm{d}^2}{\mathrm{d}\rho^2}A_2(u_h,v_h)+\frac{\mathrm{d}}{\mathrm{d}\rho}A_1(u_h,v_h)+A_0(u_h,v_h)=0\quad\forall v_h\in W_h, \tag{2.25}$$

$$u_h|_{\rho=0}=u_h^0(\phi), \tag{2.26}$$

$$u_h\text{ is bounded}\quad\text{when }\rho\to-\infty, \tag{2.27}$$

where $u_h^0(\phi)\in W_h$ and $u_h^0(\phi_j)=u^0(\phi_j)$ for $j=1,2,\ldots,M$. Suppose that $\{N^j(\phi),\ j=1,2,\ldots,M\}$ is a basis of the finite-dimensional space W_1^h such that $N^j(\phi_i)=\delta_{ij}$, $1\leqslant i,j\leqslant M$. Let

$$N(\phi)=\begin{bmatrix}N^1(\phi) & N^2(\phi) & \cdots & N^M(\phi) & 0 & 0 & \cdots & 0\\ 0 & 0 & \cdots & 0 & N^1(\phi) & N^2(\phi) & \cdots & N^M(\phi)\end{bmatrix}^{\mathrm{T}}. \tag{2.28}$$

Then for $u_h(\rho,\phi) \in V_h$, we have that

$$u_h(\rho,\phi) = \begin{pmatrix} u_1^h(\rho,\phi) \\ u_2^h(\rho,\phi) \end{pmatrix} = N^{\mathrm{T}}(\phi)U(\rho), \tag{2.29}$$

where

$$U_\rho = [u_1^h(\rho,\phi_1),\ldots,u_1^h(\rho,\phi_M),\ u_2^h(\rho,\phi_1),\ldots,u_2^h(\rho,\phi_M)]^{\mathrm{T}}. \tag{2.30}$$

Thus the problem (2.25)–(2.27) is equivalent to the following boundary value problem of a system of ordinary differential equations:

$$B_2U''(\rho) + B_1U'(\rho) + B_0U(\rho) = 0, \quad -\infty < \rho < 0, \tag{2.31}$$

$$U|_{\rho=0} = U_0, \tag{2.32}$$

$$U \text{ is bounded} \quad \text{when } \rho \to -\infty, \tag{2.33}$$

where

$$U_0 = [u_1^0(\phi_1),\ldots,u_1^0(\phi_M),\ u_2^0(\phi_1),\ldots,u_2^0(\phi_M)]^{\mathrm{T}}, \tag{2.34}$$

$$B_2 = \sum_{i=1}^{n} \int_{\theta_i}^{\theta_{i+1}} \frac{N(\phi)\mathbb{K}_1(\alpha_i)N(\phi)^{\mathrm{T}}}{\sin^2(\phi-\alpha_i)}\,\mathrm{d}\phi, \tag{2.35}$$

$$B_1 = B_3 - B_3^{\mathrm{T}}, \quad B_3 = \sum_{i=1}^{n} \int_{\theta_i}^{\theta_{i+1}} \frac{N(\phi)\mathbb{K}_2^i N'(\phi)^{\mathrm{T}}}{\sin(\phi-\alpha_i)}\,\mathrm{d}\phi, \tag{2.36}$$

$$B_0 = -\int_0^{2\pi} N'(\phi)\mathbb{K}_1(\phi)N'(\phi)^{\mathrm{T}}\,\mathrm{d}\phi. \tag{2.37}$$

For the $2M \times 2M$ matrices B_2, B_1 and B_0, we know that B_2 is a positive definite symmetric matrix, B_1 is an antisymmetric matrix and B_0 is a negative semi-definite symmetric matrix. We now solve the boundary value problem (2.31)–(2.33) by a direct method. Let

$$U(\rho) = e^{\gamma\rho}\xi, \tag{2.38}$$

where γ is a constant and $\xi \in \mathbb{C}^{2M}$ is to be determined. Substituting (2.38) into the equations in (2.31), we obtain the following generalized eigenvalue problem for determining γ and ξ:

$$[\gamma^2 B_2 + \gamma B_1 + B_0]\xi = 0. \tag{2.39}$$

Let $\eta = \gamma\xi$, then the eigenvalue problem (2.39) is reduced to the following standard eigenvalue problem:

$$\begin{pmatrix} 0 & I_{2M} \\ -B_0 & -B_1 \end{pmatrix}\begin{pmatrix} \xi \\ \eta \end{pmatrix} = \gamma\begin{pmatrix} I_{2M} & 0 \\ 0 & B_2 \end{pmatrix}\begin{pmatrix} \xi \\ \eta \end{pmatrix}, \tag{2.40}$$

where I_{2M} denotes the $2M \times 2M$ unit matrix. After solving the eigenvalue problem (2.40), we get the eigenvalues γ_j $(j = 1,2,\ldots,2M)$ with nonnegative real part and the corresponding eigenvectors

$$\begin{pmatrix} \xi_j \\ \eta_j \end{pmatrix} \quad j = 1,2,\ldots,2M$$

and $\lambda_1 = \lambda_2 = 0$, $\xi_1 = (1,\ldots,1,0,\ldots,0)^{\mathrm{T}} \in \mathbb{R}^{2M}$, $\xi_2 = (0,\ldots,0,1,\ldots,1)^{\mathrm{T}} \in \mathbb{R}^{2M}$. Particularly we suppose that γ_j $(1 \leqslant j \leqslant 2r)$ are real eigenvalues and γ_j $(2r+1 \leqslant j \leqslant 2M)$ are complex eigenvalues with nonzero imaginary parts such that $\gamma_{2l} = \bar{\gamma}_{2l-1}$ $(r+1 \leqslant l \leqslant M)$. Thus we have that

$$U(\rho) = \sum_{j=1}^{2r} b_j e^{\rho\gamma_j}\xi_j + \sum_{j=r+1}^{M} \left[b_{2j-1}\mathrm{Re}(e^{\rho\gamma_{2j}}\xi_{2j}) + b_{2j}\mathrm{Im}(e^{\rho\gamma_{2j}}\xi_{2j})\right], \tag{2.41}$$

where $\mathrm{Re}(\gamma)$ and $\mathrm{Im}(\gamma)$ denote the real part and the imaginary part of the complex number γ. Then we know that $U(\rho)$ satisfies the ordinary equation (2.31) and the boundary condition (2.33). By the condition $U(0) = U_0$, we have that

$$U_0 = \sum_{j=1}^{2r} b_j\xi_j + \sum_{j=r+1}^{M} \left[b_{2j-1}\mathrm{Re}(\xi_{2j}) + b_{2j}\mathrm{Im}(\xi_{2j})\right]. \tag{2.42}$$

Introduce matrices

$$G(\rho) = [e^{\rho\gamma_1}\xi_1, \ldots, e^{\rho\gamma_{2r}}\xi_{2r}, \mathrm{Re}(e^{\rho\gamma_{2r+2}}\xi_{2r+2}), \mathrm{Im}(e^{\rho\gamma_{2r+2}}\xi_{2r+2}), \ldots, \mathrm{Re}(e^{\rho\gamma_{2M}}\xi_{2M}), \mathrm{Im}(e^{\rho\gamma_{2M}}\xi_{2M})], \tag{2.43}$$

$$G_0 \equiv G(0) = [\xi_1, \ldots, \xi_{2r}, \mathrm{Re}(\xi_{2r+2}), \mathrm{Im}(\xi_{2r+2}), \ldots, \mathrm{Re}(\xi_{2M}), \mathrm{Im}(\xi_{2M})], \tag{2.44}$$

$$B = [b_1, b_2, \ldots, b_{2M}]^{\mathrm{T}}.$$

From (2.42), we obtain

$$B = G_0^{-1}U_0. \tag{2.45}$$

Inserting (2.45) into (2.41) we get

$$U(\rho) = G(\rho)G_0^{-1}U_0. \tag{2.46}$$

Finally, we get a semi-discrete approximate solution of problem (2.25)–(2.27):

$$u_h(\rho, \phi) = N(\phi)^{\mathrm{T}}G(\rho)G_0^{-1}U_0. \tag{2.47}$$

Substituting (2.47) into (2.10) and (2.11) we have that

$$\begin{pmatrix} X_n \\ Y_n \end{pmatrix}_{\Gamma_e} = \frac{1}{\rho_i}\mathbb{K}_1(\alpha_i)N(\phi)^{\mathrm{T}}G'(0)G_0^{-1}U_0 + \frac{\sin(\phi-\alpha_i)}{\rho_i}\mathbb{K}_2^i N'(\phi)^{\mathrm{T}}U_0, \quad \theta_i \leqslant \phi \leqslant \theta_{i+1}. \tag{2.48}$$

The equality (2.48) is a discrete artificial boundary condition at the artificial boundary Γ_i. Since this boundary condition is obtained by imposing the continuity of displacement and normal stress at Γ_i, thus it is a natural boundary condition. This boundary condition can also be viewed as an approximation of the exact boundary condition satisfied by the exact solution of the problem (1.1)–(1.3). Since the exact solution has no singularity in the domain Ω_e, thus although the corners of the polygon Γ_i are re-entrant corners in the computational domain Ω_e, they do not produce additional (artificial) singularities. This is demonstrated by our numerical results, i.e., no loss of accuracy happens.

3. The finite element approximation

On the domain Ω_e, we consider the finite element approximation of the problem (1.1)–(1.3) using the discrete artificial boundary condition (2.48) at the given artificial boundary Γ_i. Let $H^1(\Omega_i)$ denote the usual Sobolev space on Ω_i and suppose that

$$V_g = \left\{v = (v_1, v_2)^{\mathrm{T}} \in [H^1(\Omega_i)]^2 : v|_{\Gamma_1} = g\right\},$$

$$V_0 = \left\{v = (v_1, v_2)^{\mathrm{T}} \in [H^1(\Omega_i)]^2 : v|_{\Gamma_1} = 0\right\}.$$

Let $\mathscr{T}^h$ be a regular triangulation of Ω_e such that the nodes on the boundary Γ_i are mapped onto the points $(0, \phi_j)$, $j = 1, 2, \ldots, M$ by the transformation (2.5). Furthermore, we introduce the finite element subsets V^h and V_g^h

$$V^h = \left\{ v_h = (v_1^h, v_2^h)^{\mathrm{T}} : v_j^h \in C^{(0)}(\bar{\Omega}_e) \text{ and } v_j^h|_T \in P_1(T)\ \forall T \in \mathscr{T}^h,\ j = 1, 2 \right\},$$

$$V_g^h = \{ v_h \in V^h : v_h(d_j) = g(d_j) \text{ for the node } d_j \in \Gamma_1 \},$$

$$V_0^h = \{ v_h \in V^h : v_h|_{\Gamma_1} = 0 \}.$$

Then the finite element approximation of the problem (1.1)–(1.3) is:

Find $u_h \in V_g^h$ such that

$$a(u_h, v_h) + b_h(u_h, v_h) = f(v_h) \quad \forall v_h \in V_0^h, \tag{3.1}$$

where

$$a(u, v) = \int_{\Omega_i} \left[\lambda \operatorname{div} u \operatorname{div} v + 2\mu \left(\frac{\partial u_1}{\partial x_1} \frac{\partial v_1}{\partial x_1} + \frac{\partial u_2}{\partial x_2} \frac{\partial v_2}{\partial x_2} \right) + \mu \left(\frac{\partial u_1}{\partial x_2} + \frac{\partial u_2}{\partial x_1} \right) \left(\frac{\partial v_1}{\partial x_2} + \frac{\partial v_2}{\partial x_1} \right) \right] \mathrm{d}x, \tag{3.2}$$

$$b_h(u^h, v^h) = -\int_{\Gamma_i} \left[X_n(u_h) v_1^h + Y_n(u_h) v_2^h \right] \mathrm{d}s = -\sum_{i=1}^{n} \int_{\theta_i}^{\theta_{i+1}} \frac{-\rho_i}{\sin^2(\phi - \alpha_i)} \left[X_n(u_h) v_1^h + Y_n(u_h) v_2^h \right] \mathrm{d}\phi, \tag{3.3}$$

$$f(v) = \int_{\Omega_i} v^{\mathrm{T}} f \, \mathrm{d}x + \int_{\Gamma_2} v^{\mathrm{T}} q \, \mathrm{d}s. \tag{3.4}$$

Since (2.48) and we use

$$u_h|_{\tilde{\Gamma}_i} = N(\phi)^{\mathrm{T}} u_e^h, \quad v_h|_{\tilde{\Gamma}_i} = N(\phi)^{\mathrm{T}} v_e^h, \tag{3.5}$$

with

$$u_e^h = \left[u_1^h(0, \phi_1), \ldots, u_1^h(0, \phi_M),\ u_2^h(0, \phi_1), \ldots, u_2^h(0, \phi_M) \right]^{\mathrm{T}}, \tag{3.6}$$

$$v_e^h = \left[v_1^h(0, \phi_1), \ldots, v_1^h(0, \phi_M),\ v_2^h(0, \phi_1), \ldots, v_2^h(0, \phi_M) \right]^{\mathrm{T}}. \tag{3.7}$$

Then from (2.48), (3.8) and (3.5) we have that

$$\begin{aligned} b_h(u_h, v_h) &= (v_e^h)^{\mathrm{T}} \sum_{i=1}^{n} \int_{\theta_i}^{\theta_{i+1}} \left[\frac{N(\phi) \mathbb{K}_1(\alpha_i) N(\phi)^{\mathrm{T}} G'(0) G_0^{-1}}{\sin^2(\phi - \alpha_i)} + \frac{N(\phi) \mathbb{K}_2^i N'(\phi)^{\mathrm{T}}}{\sin(\phi - \alpha_i)} \right] \mathrm{d}\phi\, u_e^h \\ &= (v_e^h)^{\mathrm{T}} \left(B_2 G'(0) G_0^{-1} + B_3 \right) u_e^h \equiv (v_e^h)^{\mathrm{T}} \mathbb{K}^b u_e^h, \end{aligned} \tag{3.8}$$

where $\mathbb{K}^b = B_2 G'(0) G_0^{-1} + B_3$ denotes the stiffness matrix related to the bilinear form $b_h(\cdot, \cdot)$ or the discrete artificial boundary condition (2.48).

For the bilinear form $b_h(u_h, v_h)$, we have that

Lemma 3.1. *The bilinear form $b_h(u_h, v_h)$ is bounded and symmetric on $V^h \times V^h$. Furthermore, $b_h(v_h, v_h) \geqslant 0$ for all $v_h \in V^h$.*

Proof. From the definition of $b_h(u_h, v_h)$, we know that $b_h(u_h, v_h)$ is a bounded bilinear form on $V^h \times V^h$. For given $u_h, v_h \in V^h$, noting (3.5), we have that

$$u_h|_{\tilde{\Gamma}_i} = N(\phi)^{\mathrm{T}} u_e^h, \quad v_h|_{\tilde{\Gamma}_i} = N(\phi)^{\mathrm{T}} V_e^h. \tag{3.9}$$

On the domain $\tilde{\Omega}_i$, let

$$u_h = N(\phi)^{\mathrm{T}} G(\rho) G_0^{-1} u_e^h, \quad v_h = N(\phi)^{\mathrm{T}} G(\rho) G_0^{-1} v_e^h. \tag{3.10}$$

Thus we have the continuous extensions of u_h and v_h on $\tilde{\Omega}_i$ (say Ω_i). Let

$$D(u_h, v_h) = \int_{\Omega_i} \left[\lambda \operatorname{div} u_h \operatorname{div} v_h + 2\mu \left(\frac{\partial u_1^h}{\partial x_1} \frac{\partial v_1^h}{\partial x_1} + \frac{\partial u_2^h}{\partial x_2} \frac{\partial v_2^h}{\partial x_2} \right) + \mu \left(\frac{\partial u_1^h}{\partial x_2} + \frac{\partial u_2^h}{\partial x_1} \right) \left(\frac{\partial v_1^h}{\partial x_2} + \frac{\partial v_2^h}{\partial x_1} \right) \right] \mathrm{d}x. \tag{3.11}$$

Then for any $u_h, v_h \in V^h$, we have on recalling (3.11), integrating by parts, noting (2.5), (2.6), (2.25) and (3.10) that

$$D(u_h, v_h) = b_h(u_h, v_h) + \int_{\tilde{\Omega}_i} \left[A_2 \left(\frac{\mathrm{d}^2 u_h}{\mathrm{d}\rho^2}, v_h \right) + A_1 \left(\frac{\mathrm{d}u_h}{\mathrm{d}\rho}, v_h \right) + A_0(u_h, v_h) \right] \mathrm{d}\rho \, \mathrm{d}\phi = b_h(u_h, v_h). \tag{3.12}$$

Hence

$$b_h(u_h, v_h) = D(u_h, v_h) = D(v_h, u_h) = b_h(v_h, u_h) \quad \forall u_h, v_h \in V^h, \tag{3.13}$$

$$b_h(v_h, v_h) = D(v_h, v_h) \geqslant 0 \quad \forall v_h \in V^h. \tag{3.14}$$

Thus it is straightforward to check that the problem (3.1) is well posed. After solving the problem (3.1) we obtain u_h, the approximate solution of the original problem (1.1)–(1.3) on the domain Ω_e. Thus we can compute the stress intensity factors directly from u_h by the method of limitation of displacement or limitation of stress [5]. Here we present the formula of the method of limitation of displacement. In fact, after solving the problem (3.1), we know the vector U_0 (see (2.34)). By solving the linear system (2.42), we get the vector B (see (2.45)). Suppose that γ_3 be the eigenvalue with smallest positive real part among all the eigenvalues of the eigenvalue problem (2.39). Then the open mode and shear mode stress intensity factors at the crack tip O can be computed

$$K_{\mathrm{I}} = \frac{\sqrt{2\pi}\mu}{\kappa + 1} \lim_{\rho \to -\infty} \mathrm{e}^{-\rho\gamma_3} [u_2(\rho, 0) - u_2(\rho, 2\pi)] = \frac{\sqrt{2\pi}\mu}{\kappa + 1} b_3 \left(\xi_{M+1,3} - \xi_{2M,3} \right), \tag{3.15}$$

$$K_{\mathrm{II}} = \frac{\sqrt{2\pi}\mu}{\kappa + 1} \lim_{\rho \to -\infty} \mathrm{e}^{-\rho\gamma_3} [u_1(\rho, 2\pi) - u_1(\rho, 0)] = \frac{\sqrt{2\pi}\mu}{\kappa + 1} b_3 \left(\xi_{M,3} - \xi_{1,3} \right), \tag{3.16}$$

where $\xi_3 = (\xi_{1,3}, \ldots, \xi_{M,3}, \xi_{M+1,3}, \ldots, \xi_{2M,3})^{\mathrm{T}}$ and $\kappa = (\lambda + 3\mu)/(\lambda + \mu)$. The formula of the method of limitation of stress can be obtained similarly. □

4. Numerical implementation

In this section, we present the numerical implementation of coupling the FEM and the direct method of lines to simulate the fracture problem. Without loss of generality, we suppose that the problem contains a single edge crack (see Fig. 1). Introducing a polygonal line artificial boundary $\Gamma_i = \overline{a_1 a_2 \cdots a_{n+1}}$, then the domain Ω is divided into two parts, Ω_i and Ω_e. Let $\mathscr{T}^h$ be a regular triangulation of Ω_e, i.e., $\bar{\Omega}_e = \cup_{K \in \mathscr{T}^h} K$, where K is a triangle. Suppose the nodes on Γ_i of the triangulation $\mathscr{T}^h$ are b_j $(x_1^j, x_2^j) = (R_j \cos\phi_j, R_j \sin\phi_j)$ for $j = 1, 2, \ldots, M$ satisfying $0 = \phi_1 < \phi_2 < \cdots < \phi_M = 2\pi$. We define the following element-level matrices on the interval $[\phi_j, \phi_{j+1}]$ for $j = 1, 2, \ldots, M-1$:

$$B_2^j = \int_{\phi_j}^{\phi_{j+1}} \frac{N_j(\phi) \mathbb{K}_1(\alpha_j) N_j(\phi)^{\mathrm{T}}}{\sin^2(\phi - \alpha_j)} \, \mathrm{d}\phi, \tag{4.1}$$

$$B_1^j = B_3^j - (B_3^j)^{\mathrm{T}}, \quad B_3^j = \int_{\phi_j}^{\phi_{j+1}} \frac{N_j(\phi) \mathbb{K}_2^j N_j'(\phi)^{\mathrm{T}}}{\sin(\phi - \alpha_j)} \, \mathrm{d}\phi, \tag{4.2}$$

$$B_0^j = -\int_{\phi_j}^{\phi_{j+1}} N_j'(\phi)\mathbb{K}_1(\phi)N_j'(\phi)^{\mathrm{T}}\,\mathrm{d}\phi, \tag{4.3}$$

where α_j is calculated by (2.4) and

$$N_j(\phi) = \begin{bmatrix} N_j^1(\phi) & N_j^2(\phi) & 0 & 0 \\ 0 & 0 & N_j^1(\phi) & N_j^2(\phi) \end{bmatrix}^{\mathrm{T}} = \begin{bmatrix} \frac{\phi_{j+1}-\phi}{\phi_{j+1}-\phi_j} & \frac{\phi-\phi_j}{\phi_{j+1}-\phi_j} & 0 & 0 \\ 0 & 0 & \frac{\phi_{j+1}-\phi}{\phi_{j+1}-\phi_j} & \frac{\phi-\phi_j}{\phi_{j+1}-\phi_j} \end{bmatrix}^{\mathrm{T}}. \tag{4.4}$$

The 4×4 matrices B_0^j, B_1^j, B_2^j and B_3^j can be obtained by numerical integration like obtaining the element-level stiffness matrix in the usual finite element method. Then the matrices B_0, B_1, B_2 and B_3 (see (2.35)–(2.37)) are obtained by assembling the element-level matrices B_0^j, B_1^j, B_2^j and B_3^j for $j = 1, 2, \ldots, M-1$, respectively. This procedure is the same as obtaining the total stiffness matrix by assembling the element-level stiffness matrices in the usual finite element method. After solving the eigenvalue problem (2.40), one gets the eigenvalues γ_j $(j = 1, 2, \ldots, 2M)$ with nonnegative real part and the corresponding eigenvectors

$$\begin{pmatrix} \xi_j \\ \eta_j \end{pmatrix}, \quad j = 1, 2, \ldots, 2M.$$

From these eigenvalues and eigenvectors, the matrices $G(\rho)$ (see (2.43)) and G_0 (see (2.44)) can be constructed easily. Thus the stiffness matrix $\mathbb{K}^b$ (see (3.8)) related to the bilinear form $b_h(\cdot,\cdot)$ can be obtained by matrix multiplication and addition. Therefore the total stiffness matrix of the problem (3.1) can be obtained by assembling the stiffness matrix $\mathbb{K}^a$ related to the bilinear form $a(\cdot,\cdot)$ and the stiffness matrix $\mathbb{K}^b$ together. The remaining calculation is the same as the usual finite element method. It is omitted here.

5. Numerical examples and results

To demonstrate the efficiency and accuracy of the present method, stress intensity factors are calculated for one problem with exact solution and two typical fracture problems.

Example 1. The fracture problem with a single edge crack tip (see Fig. 3).

Consider the problem (1.1)–(1.3) in the domain Ω (as shown in Fig. 3). We choose $\Gamma_1 = \overline{PRSTWQ}$, $\Gamma_2 = \overline{OP} \cup \overline{OQ}$, $f = 0$, $q = 0$ and $g(r,\theta) = (g_1(r,\theta), g_2(r,\theta))^{\mathrm{T}}$ (see the functions in (1.1)–(1.3)) with

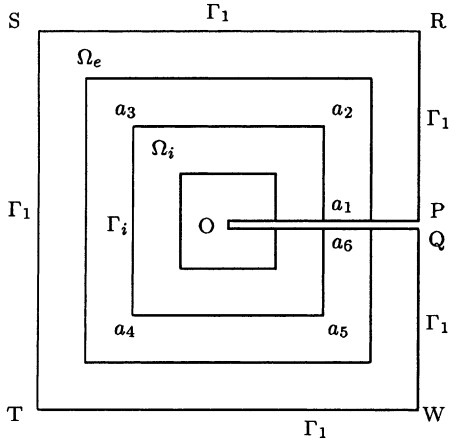

Fig. 3. Set up of Example 1 and artificial boundaries.

$$g_1(r,\theta) = -\frac{r^{1/2}}{\sqrt{8\pi\mu}}\left[a_1 \sin\frac{\theta}{2}\left(\kappa - 1 + 2\cos^2\frac{\theta}{2}\right) + a_2 \cos\frac{\theta}{2}\left(\kappa + 1 + 2\sin^2\frac{\theta}{2}\right)\right], \tag{5.1}$$

$$g_2(r,\theta) = \frac{r^{1/2}}{\sqrt{8\pi\mu}}\left[a_1 \cos\frac{\theta}{2}\left(\kappa + 1 - 2\sin^2\frac{\theta}{2}\right) - a_2 \sin\frac{\theta}{2}\left(\kappa - 1 - 2\cos^2\frac{\theta}{2}\right)\right], \tag{5.2}$$

where $\kappa = (\lambda + 3\mu)/(\lambda + \mu)$. We choose $a = |RS| = 2$, $b = |PR| = |QW| = |OP| = 1$ in Fig. 3, $a_1 = 2$, $a_2 = 2$ in (5.1) and (5.2) and the Poisson ratio $v = 0.3$. It is easy to show that the open mode and shear mode stress intensity factors at the crack tip O are $K_{\mathrm{I}} = 2$ and $K_{\mathrm{II}} = 2$ [1]. Now we use this example which has exact solution to test the effect of the mesh size of the triangulation $\mathscr{T}^h$, the shape and size of the domain surrounding the crack tip O.

First, we test the effect of the mesh size h. We choose $\Gamma_i = \overline{a_1a_2a_3a_4a_5a_6}$ as the artificial boundary. Three uniform meshes with different mesh size h for the domain Ω_e were used in this computation. Let K_{I}^h and K_{II}^h denote the numerical solutions of the stress intensity factors on the mesh with mesh size h. Table 1 shows the numerical solutions K_{I}^h and K_{II}^h and the errors $|K_{\mathrm{I}} - K_{\mathrm{I}}^h|$ and $|K_{\mathrm{II}} - K_{\mathrm{II}}^h|$ for different mesh size h.

Second, we test the effect of the size of the domain surrounding the crack tip. We choose three different artificial boundaries with the same shape but different size (see Fig. 3), respectively. The distance from the artificial boundary to the crack tip is $c = 0.25$, $c = 0.5$ and $c = 0.75$, respectively. On the domain Ω_e, we use uniform mesh with fixed mesh size $h = 0.125$. Let K_{I}^c and K_{II}^c denote the numerical solutions of the stress intensity factors with respect to the domain surrounding the crack tip with the distance c from the artificial boundary to the crack tip. Table 2 shows the numerical solutions K_{I}^c and K_{II}^c and the errors $\left|K_{\mathrm{I}} - K_{\mathrm{I}}^c\right|$ and $\left|K_{\mathrm{II}} - K_{\mathrm{II}}^c\right|$ for different sizes of the domain surrounding the crack tip.

Third, we test the shape of the artificial boundary. We choose three different shapes of the artificial boundary (as shown in Fig. 4): $\Gamma_i^1 = \overline{a_1a_2a_3a_4a_5a_6}$, $\Gamma_i^2 = \overline{a_1b_1b_2b_3b_4b_5b_6b_7b_8a_6}$ and $\Gamma_i^3 = \overline{a_1c_1c_2c_3a_6}$, respectively. On the domains Ω_e, we use uniform mesh with a fixed mesh size $h = 0.125$, respectively. Let K_{I}^j and K_{II}^j denote the numerical solutions of the stress intensity factors by using the artificial boundary Γ_i^j $(j = 1, 2, 3)$. Table 3 shows the numerical solutions K_{I}^j and K_{II}^j and the errors $\left|K_{\mathrm{I}} - K_{\mathrm{I}}^j\right|$ and $\left|K_{\mathrm{II}} - K_{\mathrm{II}}^j\right|$ for different shapes of the domain surrounding the crack tip.

From Tables 1–3, we can see that the numerical solutions converge linearly with respect to the mesh size. The shape and size of the domain surrounding the crack tip have little effect on the numerical solutions. Thus one can choose the domain Ω_i surrounding the crack tip as large as possible and satisfying the condition $f = 0$ in $\bar{\Omega}_i$. One can also choose the shape of the domain Ω_i surrounding the crack tip as he likes such that he can triangulate the domain Ω_e easily. In general, one can choose the artificial boundary Γ_i such that $0 = \theta_1 < \theta_2 < \cdots < \theta_{n+1} = 2\pi$ (see Fig. 1), where θ_i is the polar angle of the vertex a_i, be a uniform

Table 1
The numerical solutions of the stress intensity factors with different mesh size h

Mesh	K_{I}^h	$\lvert K_{\mathrm{I}} - K_{\mathrm{I}}^h\rvert$	K_{II}^h	$\lvert K_{\mathrm{II}} - K_{\mathrm{II}}^h\rvert$
$h = 0.5$	2.0449	0.0449	1.9319	0.0681
$h = 0.25$	2.0180	0.0180	1.9737	0.0263
$h = 0.125$	2.0096	0.0096	2.0086	0.0086

Table 2
The numerical solutions of the stress intensity factors with different size of the domain surrounding the crack tip

Mesh	K_{I}^c	$\lvert K_{\mathrm{I}} - K_{\mathrm{I}}^c\rvert$	K_{II}^c	$\lvert K_{\mathrm{II}} - K_{\mathrm{II}}^c\rvert$
$c = 0.25$	2.0069	0.0069	1.9960	0.0040
$c = 0.5$	2.0096	0.0096	2.0086	0.0086
$c = 0.75$	2.0083	0.0083	1.9916	0.0084

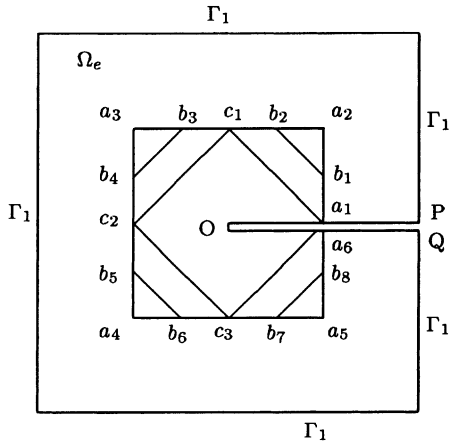

Fig. 4. Different shapes of artificial boundaries in Example 1.

Table 3
The numerical solutions of the stress intensity factors with different shape of the domain surrounding the crack tip

Mesh	K_{I}^j	$\lvert K_{\mathrm{I}} - K_{\mathrm{I}}^j \rvert$	K_{II}^j	$\lvert K_{\mathrm{II}} - K_{\mathrm{II}}^j \rvert$
$j = 1$	2.0096	0.0096	2.0086	0.0086
$j = 2$	2.0006	0.0006	1.9942	0.0058
$j = 3$	1.9991	0.0009	2.0077	0.0077

partition of the interval $[0, 2\pi]$. Choosing Γ_i in this way is to reduce the error that comes from the discretization of the problem (2.19)–(2.21).

Example 2. A typical fracture problem with a single edge crack tip (see Fig. 5) [5,6].

We introduce the artificial boundary $\overline{OABCDEF}$ around the crack tip O and choose $p = 1$, $w = 2$, $s = 8$, $a = 1$ and the Poisson ratio $v = 0.3$ in this example (see Fig. 5). Using symmetry conditions, only half of the domains are needed in our computation. Let K_{I} and K_{II} be the open mode and shear mode stress intensity factors at the crack tip. It is easy to see that the shear mode stress intensity factor K_{II} is zero in this example because of the symmetry of the problem. Four uniform meshes with different mesh size h for the domain Ω_e were used in our computation. As we do not have the exact solution for this problem, we use the numerical solution at the finest mesh as the "exact solution" K_{I} to compare with our numerical results. The numerical solutions of the stress intensity factors are given in Table 4. Furthermore several approximate eigenvalues of the problem (2.40) for this example are given in Table 5. From Table 4, we can see the numerical solution converges linearly. This result agrees with the error estimation for the usual finite element method.

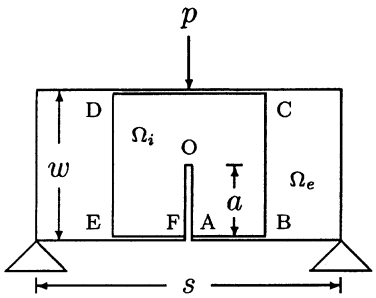

Fig. 5. Set up of Example 2 and artificial boundary.

Table 4
The approximate stress intensity factors at the crack tip O in Example 2[a]

Mesh	K_I^h	$\lvert K_I - K_I^h\rvert$	$K_I^{N,h}$	$\lvert K_I^N - K_I^{N,h}\rvert$
$h = 1$	13.4384	3.1530	9.5024	2.2295
$h = 0.5$	15.2224	1.3690	10.7639	0.9680
$h = 0.25$	16.2482	0.3432	11.4892	0.2427
$h = 0.125$	16.5914		11.7319	

[a] Here K_I^N denotes the normalized open mode stress intensity factor and $K_I^{N,h}$ denotes its numerical approximation.

Table 5
Several approximate eigenvalues in Example 2

Mesh	$h = 1$	$h = 0.5$	$h = 0.25$	Exact value
γ_3	0.48309	0.49632	0.499098	0.5
γ_5	1.1899+0.0545i	1.0264	1.0065	1.0
γ_7	1.1899 −0.0545i	1.4421	1.4859	1.5

Example 3. A typical fracture problem with two edge crack tips (see Fig. 6) [24].

We introduce two distinct artificial boundaries $\overline{O_1A_1B_1C_1D_2E_1F_1}$ and $\overline{O_2A_2B_2C_2D_2E_2F_2}$ around the crack tips O_1 and O_2, respectively (see Fig. 6). We choose $p = 1$, $|O_1A_1| = a_1 = 1.0$, $|O_2A_2| = a_2 = 0.5$, $s = 2$, $w = 2$ and the Poisson ratio $v = 0.3$ in our computation. Using symmetry conditions, only half of the domain is needed in our computation. Let K_I and K_{II} be the open mode and shear mode stress intensity factors at the crack tip. It is easy to see that the shear mode stress intensity factor K_{II} is zero in this example because of the symmetry of the problem. Three uniform meshes with different mesh size h for the domain Ω_e were used in our computation. The numerical results for the stress intensity factors are given in Table 6. The

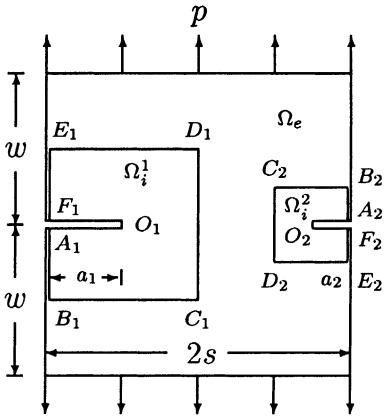

Fig. 6. Set up of Example 3 and artificial boundaries.

Table 6
The approximate stress intensity factors at the crack tips O_1 and O_2 in Example 3

Mesh	$h = 0.5$	$h = 0.25$	$h = 0.125$
K_I^h at the crack tip O_1	1.0684	1.1131	1.1257
K_I^h at the crack tip O_2	2.7614	2.8059	2.8183

results shown in Tables 4 and 6 agree very well with the results in the previous results in [5,6] and in the handbooks of stress intensity factors [24].

6. Discussion and conclusions

By coupling the FEM and the direct method of lines, we propose a method to calculate the stress intensity factor in fracture problems with cracks. The present method can overcome the loss of accuracy of the standard finite element approximation for fracture problems with cracks. This method need not know previously the singularity at the crack tip. In fact it can compute the singularity numerically and easily couple with the usual finite element method. Thus one can easily apply it to compute practical fracture problems, such as composite materials. Although only the formulation for linear finite element is presented, it is obvious that other high order finite elements can be formulated in a similar manner.

A fracture problem with exact solution and two typical plane fracture problems were computed by the present method. The numerical results show linear convergence rate with respect to the mesh size when using the linear finite element and the shape and size of the domain surrounding the crack tip have little effect. Thus one can choose the shape and size of the domain surrounding the crack tip arbitrarily. In general, one can choose the domain Ω_i surrounding the crack tip as large as possible and satisfying the condition $f = 0$ in $\bar{\Omega}_i$. The artificial boundary Γ_i is chosen such that $0 = \theta_1 < \theta_2 < \cdots < \theta_{n+1} = 2\pi$ (see Fig. 1), where θ_i is the polar angle of the vertex a_i, be a uniform partition of the interval $[0, 2\pi]$. The numerical results also match very well to previous computations. Thus numerical results demonstrate the efficiency and accuracy of the present method.

Acknowledgements

This work was supported partly by the Climbing Program of National Key Project of Foundation and the National Natural Science Foundation of China. Computation was supported by the State Key Laboratory of Scientific and Engineering Computing in China.

References

[1] M.L. Williams, Stress singularities resulting from various loading conditions in angular corners of plates in extension, J. Appl. Mech. 19 (1952) 526–528.
[2] A. Holston, A mixed mode crack tip finite element, Int. J. Fracture 12 (1976) 887–899.
[3] C.W. Cai, M.J. Liu, C.M. Huang, An arbitrarily high order singular stain finite element for calculating the stress intensity factors in plate problems, Acta Mech. Sol. Sinica 4 (1983) 597–605.
[4] R.W. Thatcher, The use of infinite grid refinement at singularities in the solution of Laplace's equation, Numer. Math. 25 (1976) 163–178.
[5] L. Ying, The infinite similar element method for calculating stress intensity factors, Sci. Sinica 6 (1977) 517–535.
[6] H. Han, L. Ying, An iterative method in the infinite element, Math. Numer. Sinica 1 (1979) 91–99.
[7] I. Babuska, M.B. Rosenzweig, A finite element scheme for domains with corners, Numer. Math. 20 (1972) 1–21.
[8] J.E. Akin, Generation of elements with singularities, Int. J. Numer. Methods Engrg. 10 (1976) 1249–1259.
[9] J.R. Whiteman, J.E. Akin, Finite elements, singularities and fracture, in: J.R. Whiteman (ed.), The Mathematics of Finite Elements and Applications III, MAFELAP 1978, Academic Press, London, 1979, pp. 35–54.
[10] Y.K. Cheung, C.P. Jiang, Application of the finite strip method to plane fracture problems, Engrg. Frac. Mech. 53 (1996) 89–96.
[11] D. Givoli, L. Rivkin, J.B. Keller, A finite element scheme for domains with corners, Int. J. Numer. Methods Engrg. 35 (1992) 1329–1345.
[12] D. Givoli, S. Vigderganz, Finite element analysis of wave scattering from singularities, Wave Motion 20 (1994) 165–176.
[13] D. Givoli, L. Rivkin, The DtN finite element method for elastic domains with cracks and re-entrant corners, Comput. Struct. 49 (1993) 633–642.
[14] X. Wu, H. Han, A finite-element method for Laplace and Helmholtz type boundary value problems with singularities, SIAM J. Numer. Anal. 34 (1997) 1037–1050.
[15] W. Bao, H. Han, The direct method of lines for the problem of infinite elastic foundation, Comput. Methods Appl. Mech. Engrg. 75 (1999) 157–173.

[16] H. Han, W. Bao, The discrete artificial boundary condition on a polygonal artificial boundary for the exterior problem of Poisson equation by using the direct method of lines, Comput. Methods Appl. Mech. Engrg. 179 (1999) 345–360.
[17] H. Han, W. Bao, An artificial boundary condition for two-dimensional incompressible viscous flows using the method of lines, Int. J. Numer. Methods Fluids 22 (1996) 483–493.
[18] H. Han, W. Bao, An artificial boundary condition for the incompressible viscous flows in a no-slip channel, J. Comput. Math. 13 (1995) 51–63.
[19] O.C. Zienkiewicz, C. Emson, P. Bettess, A novel boundary infinite element, Int. J. Numer. Methods Engrg. 19 (1983) 393–404.
[20] H. Han, W. Bao, T. Wang, Numerical simulation for the problem of infinite elastic foundation, Comput. Methods Appl. Mech. Engrg. 147 (1997) 369–385.
[21] W. Bao, H. Han, Nonlocal artificial boundary conditions for the incompressible viscous flow in a channel using spectral techniques, J. Comput. Phys. 126 (1996) 52–63.
[22] L.S. Xanthis, C. Schwab, The method of arbitrary lines, C.R. Acad. Sci. Paris 312 Serie I (1991) 181–187.
[23] D. Givoli, Numerical Methods for Problems in Infinite Domains, Elsevier, Amsterdam, 1992.
[24] G.C. Sih, Handbook of Stress Intensity Factors for Researchers and Engineers, Leheigh University, Bethlehem, PA. USA, 1973.